Complex Wavelet Transforms with Allpass Filters

Felix C. A. Fernandes, and Ivan W. Selesnick, Rutger L. C. van Spaendonck, C. Sidney Burrus

December 18, 2002

Texas Instruments
DSPS R&D Cr., Texas Instruments, Dallas, TX, USA

Electrical Engineering, Polytechnic University
6 Metrotech Center, Brooklyn, NY 11201, USA
selesi@poly.edu
tel: 718 260-3416
fax: 718 260-3906

Rice University
Electrical and Computer Engineering
Houston, TX, USA

Abstract

Complex discrete wavelet transforms have significant advantages over real wavelet transforms for certain signal processing problems. Two approaches to the implementation of complex wavelet transforms have been proposed earlier. Both approaches require discrete-time allpass systems having approximately linear-phase and (fractional) delay. This paper compares the results when different allpass systems are used. In the earlier work, maximally flat delay allpass systems were used. In this paper, it is shown that an allpass system designed according to the minimax criterion yields improvements for the complex discrete wavelet transforms.

1 Introduction

Although the Discrete Wavelet Transform (DWT) is a powerful signal-processing tool, it has three disadvantages that undermine its usage in many applications. First, it is shift sensitive because input-signal shifts generate unpredictable changes in DWT coefficients. Second, the DWT suffers from poor directionality because DWT coefficients reveal only three spatial orientations. Third, DWT analysis of real signals lacks the phase information that accurately describes non-stationary signal behavior. To overcome these problems, Kingsbury [20, 19] created the Dual-Tree Wavelet Transform (DTWT), a redundant, complex wavelet transform with excellent directionality, reduced shift sensitivity and explicit phase information. Because of these advantages, the DTWT yields excellent results in applications where redundancy is acceptable [6, 32]. The DTWT is redundant because it consists of a pair of filter banks that simultaneously operate on the input signal and provide two wavelet decompositions. The wavelets associated with the filter banks are a Hilbert pair. This property is critical since it provides the advantages of reduced shift sensitivity, improved directionality and explicit phase information. However, the design of Kingsbury's DTWT filters is complicated because it requires an iterative optimization over the space of perfect-reconstruction filter banks.

To simplify and generalize the DTWT design procedure, Selesnick [40, 41] proposed a new method to obtain filters that may be used in a DTWT. He demonstrated that arbitrary-length DTWT filters with specified number of vanishing moments may be generated from the spectral factorization of a certain halfband filter. In addition, he proved that the wavelets associated with the DTWT are a Hilbert pair if the halfband filter has a fractional-delay allpass factor. Selesnick's technique applies to the design of orthogonal, biorthogonal and IIR DTWTs.

A limitation of the DTWT approach to complex wavelet transform implementation is that the DTWT is redundant because transform coefficients require more storage space than the input signal. This disadvantages the DTWT since redundant transforms cannot be used in applications such as image/video compression where parsimonious signal representations are crucial. To overcome this disadvantage Fernandes et al. [8] subsequently defined projection-based Complex Wavelet Transforms (CWTs), a new framework for the implementation of complex wavelet transforms. In this framework, the input signal is projected onto a signal-space so that its real and imaginary parts form a Hilbert pair. The complex wavelet transform is then implemented by computing the DWT of the projected signal. Because the redundancy of the projection may be controlled explicitly, both redundant as well as non-redundant complex wavelet transforms are obtainable. The projection filters that implement orthogonal, non-redundant CWTs must be generated by the modulation of

a lowpass filter that is the sum of allpass polyphase components with fractional delay.

In this paper, we shall first briefly explain the theory behind fractional-delay allpass filters. Then we shall describe the projection-based and DTWT approaches to the implementation of complex wavelet transforms. In each case, we shall show that minimax allpass filters provide better performance than maximally flat allpass filters.

2 Fractional-Delay Allpass Systems

The procedures presented in this paper for the design and implementation of complex discrete wavelet transforms (DWT) depend on the design of allpass systems. Specifically, the projection-based complex DWT described in Section 3 requires the design of a (modulated) lowpass filter realized as the sum of two allpass systems,

$$H(z) = A_0(z^2) + z^{-1}\, A_1(z^2). \tag{1}$$

Section 4 requires the design of an allpass system that approximates a delay of 0.5 samples.

The design of a lowpass filters realizable as a sum of allpass systems has been described in several papers [37, 34, 1, 2, 15, 25, 31, 33, 35]. It turns out, that the design of the lowpass filter in (1) requires again an allpass system that approximates a fractional delay. Therefore, the design of such an allpass system is common to both types of complex DWTs described below.

The allpass system $A(z)$ has the frequency response $e^{j\,\theta(\omega)}$ and it is desired that the phase response $\theta(\omega)$ approximates the linear function of frequency: $\theta(\omega) \approx -\tau\,\omega$. There are several methods to design allpass systems with general phase responses [4, 10, 17, 18, 24, 26, 27, 28, 29, 36, 48] but the earlier implementations of complex DWT of [41, 8] employ allpass systems designed according to the maximally-flat criterion [9, 14, 43, 46, 21]. However, as will be illustrated in Sections 3 and 4, the complex DWTs can be improved by using allpass systems designed according to the minimax (or Chebyshev) design criterion. In this case, an allpass system $A(z)$ is sought so as to minimize the maximum of the (weighted) error function,

$$\max_{|\omega|\leq 0.5\,\pi} |\theta(\omega) + \tau\,\omega|.$$

For this approximation problem, several authors has presented iterative Remez-like exchange algorithms for the design of allpass filters and allpass sums according to the Chebyshev criterion [11, 16, 22, 23, 38, 36]. In the examples presented below, we used Matlab programs by Lang and Schüßler that are available on the web at `http://www-nt.e-technik.uni-erlangen.de/~hws/programs/halfbandfilters/` and at

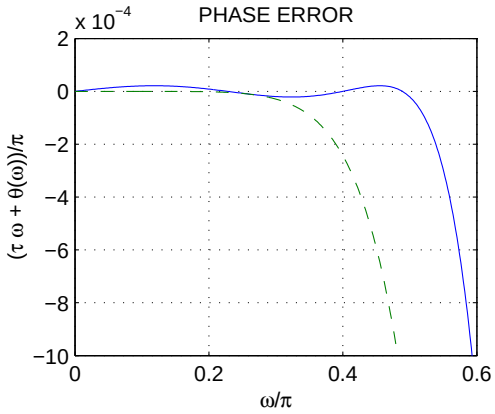

Figure 1: Allpass system.

`http://www.dsp.rice.edu/software/allpass.shtml`. Figure 1 illustrates the error functions of allpass systems designed according to the maximally-flat and minimax criteria.

3 Projection-Based Complex Wavelet Transforms

In 1999, Kingsbury [20] developed the Dual-Tree Wavelet Transform (DTWT), a complex wavelet transform that has improved directionality and reduced shift sensitivity when compared to the Real Wavelet Transform (RWT [1]) [3]. One explanation for the DTWT advantages is that the DTWT coefficients may be related to an analysis obtained from the DWT associated with an analytic[2] wavelet [7]. In 2000, Fernandes et al. [8] devised a different method to obtain complex wavelet coefficients that may also be related to DWT analysis with an analytic wavelet. They argued that such an analysis may be performed on $L^2(\mathbb{R} \to \mathbb{R})$[3] signals by first projecting the input signal onto the Hardy space[4] and then computing its wavelet transform using the DWT associated with a real wavelet. Fernandes [7] proved that these projection-based Complex Wavelet Transforms (CWTs)

[1] The acronym RWT (Real Wavelet Transform) refers specifically to the DWT of a real-valued function. Since we consider only DWTs implemented with real filters, RWT coefficients are always real.

[2] Analytic functions have frequency responses that vanish over negative frequencies.

[3] Usually, the notation $L^2(\mathbb{R})$ represents the space of square-integrable, complex-valued functions on the real line. To differentiate between complex-valued and real-valued functions, we shall denote this functional space by $L^2(\mathbb{R} \to \mathbb{C})$ and we shall use the notation $L^2(\mathbb{R} \to \mathbb{R})$ to represent the subspace of $L^2(\mathbb{R} \to \mathbb{C})$ that is comprised of real-valued functions.

[4] The classical Hardy space $H^2(\mathbb{R} \to \mathbb{C})$ is defined by
$H^2(\mathbb{R} \to \mathbb{C}) \triangleq \{f \in L^2(\mathbb{R} \to \mathbb{C}) : F(\omega) = 0 \text{ for a.e. } \omega < 0, \text{ where } F \text{ is the Fourier transform of } f\}$.

also improve directionality and have reduced shift sensitivity when compared to the RWT. One advantage of the projection-based approach over the DTWT approach is that transform redundancy may be controlled explicitly by selecting between redundant and non-redundant projection methods. In particular, the projection-based framework allows for the creation of directional, non-redundant complex wavelet transforms with potential benefits for video/image coding systems.

In this section, we shall first explain the redundant, projection-based complex wavelet transform. Next we shall show how the projection can be made non-redundant to implement a non-redundant complex wavelet transform. This non-redundant complex wavelet transform is orthogonal if and only if allpass filters are used in the projection stage. We compare the performance of maximally flat allpass filters and minimax allpass filters in the projection stage and we shall demonstrate that the minimax allpass filters provide better directionality than the maximally flat allpass filters.

3.1 The Redundant Complex Wavelet Transform

In [7], Fernandes explained why the DWT of the Hardy-space projection of an $L^2(\mathbb{R} \to \mathbb{R})$ function has more directionality, phase information and shift insensitivity than the DWT of the function itself. However, since it is impossible to compute such a projection, he defined the Softy space, a new function space that approximates the Hardy space. The redundant Complex Wavelet Transform (CWT) of an $L^2(\mathbb{R} \to \mathbb{R})$ function is defined to be the DWT of its Softy-space projection, as depicted in Figure 2. The projection filter h^+ is used to project an $L^2(\mathbb{R} \to \mathbb{R})$ function f onto the Softy space. This filter has a passband over $[0, \pi]$ and a stopband over $(-\pi, 0)$ so that it retains positive frequencies and suppresses negative frequencies. The filtering implements a projection onto an approximation to Hardy space because Hardy-space functions vanish over negative frequencies. Next, we compute f_d^+, the DWT of the Softy-space projection f^+. We define f_d^+ to be the projection-based, redundant CWT. This function will then undergo application-specific processing followed by an Inverse DWT (IDWT). An inverse-projection filter g^+ returns the $L^2(\mathbb{R} \to \mathbb{R})$ processed function $\hat{f}$.

As shown in Fig. 3, the filter bank that computes the CWT is easily implemented by passing c, the scaling coefficient sequence associated with f, through the projection filter h^+ before feeding it to a DWT filter bank. After application-specific processing, the inverse CWT is implemented with the inverse DWT followed by an inverse projection filter g^+, where $H^+(z)G^+(z)$ is a halfband filter satisfying certain conditions [7, Pg. 23].

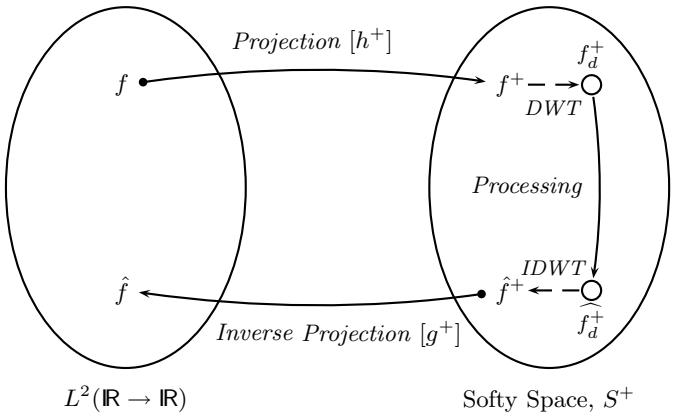

Figure 2: f^+ is the Softy-space projection of f, and f_d^+ is the Complex Wavelet Transform (CWT) of f.

3.2 The Non-Redundant CWT

In the preceding section, we introduced the CWT as the DWT of f^+, the Softy-space projection of an $L^2(\mathbb{R} \to \mathbb{R})$ function f. Since f^+ approximates f^H, the Hardy-space projection of f, the CWT exhibits explicit phase information, reduced shift sensitivity and improved directionality. The reduced shift sensitivity is obtained at the expense of a small amount of data redundancy introduced by the projection filter. The redundancy is incurred because the projection of a real-valued signal will be complex valued in general. However, redundancy is unacceptable in applications such as data compression. Therefore, to obtain a directional, non-redundant CWT, we shall now develop the non-redundant projection: a projection that incurs no data redundancy while projecting an $L^2(\mathbb{R} \to \mathbb{R})$ function onto a function space that approximates Softy space. We shall refer to the DWT of the non-redundant projection of an $L^2(\mathbb{R} \to \mathbb{R})$ function as "the non-redundant CWT". This transform has improved directionality and offers explicit phase information. It does not however have reduced shift sensitivity. Therefore, the non-redundant CWT is targeted at applications such as data compression in which a non-redundant transform is more important than reduced shift sensitivity.

Apart from creating the non-redundant CWT, the non-redundant projection has another significant application. In [7], we demonstrate that the non-redundant projection may be used to improve

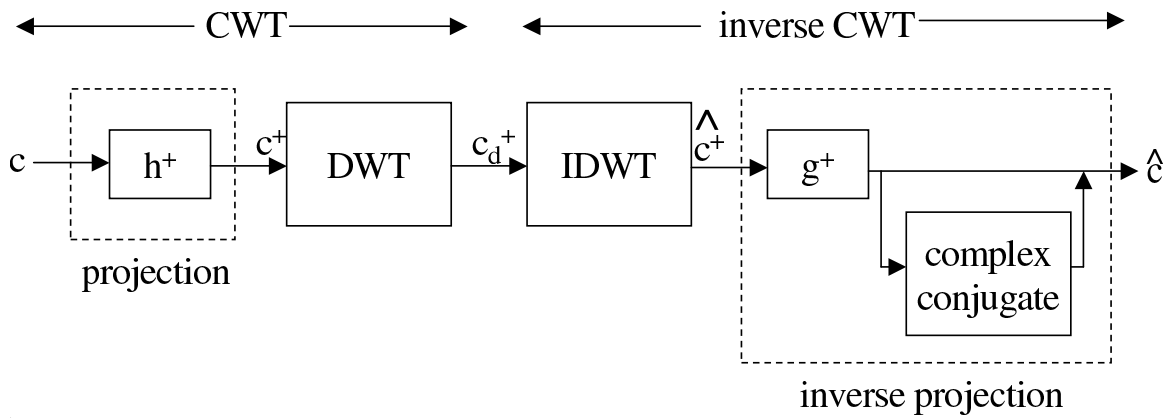

Figure 3: Filter-bank implementation of the Redundant CWT and its Inverse

transforms such as the undecimated DWT and the Double-Density DWT [42]. We achieve the improvement by enhancing directionality and providing useful phase information without increasing redundancy and while preserving shift-invariance properties.

3.2.1 Defining the Non-Redundant Projection

In Section 3.1 we used the projection filter h^+ to define the Softy-space projection of an $L^2(\mathbb{R} \to \mathbb{R})$ function. However, the complex coefficients of h^+ introduce data redundancy into the CWT. To eliminate this data redundancy which is unacceptable in certain applications, we now propose the non-redundant projection scheme shown in Fig. 4. As depicted in the figure, we define the non-

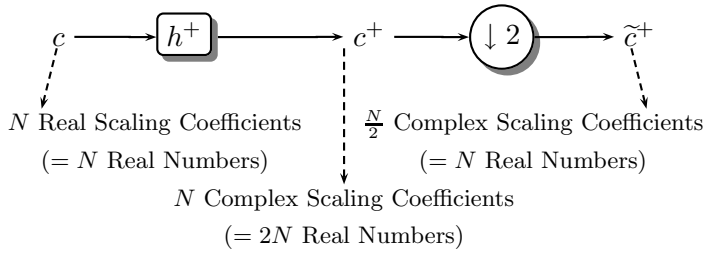

Figure 4: The non-redundant projection consists of a projection filter followed by a downsampler. This projection is non-redundant because $\widetilde{c}^+$ has the same storage requirement as c (N real numbers).

redundant projection to be the concatenation of a projection filter and a downsampler (elimination of odd-indexed scaling coefficients). The downsampler eliminates the redundancy created by the

projection filter that generates complex scaling coefficients from real scaling coefficients. Observe that the scaling-coefficient sequences c and $\widetilde{c}^+$ can both be represented by N real numbers within a digital computer; therefore, there is no data redundancy in the scaling-coefficient sequence $\widetilde{c}^+$.

In [7], we prove that the non-redundant projection of an $L^2(\mathbb{R} \rightarrow \mathbb{R})$ function with a lowpass characteristic is approximately equal to the Softy-space projection of a low resolution version of the function. This result is significant because it empowers the non-redundant projection with the directionality and phase information associated with the Softy-space projection.

3.2.2 The Non-Redundant CWT and Its Inverse

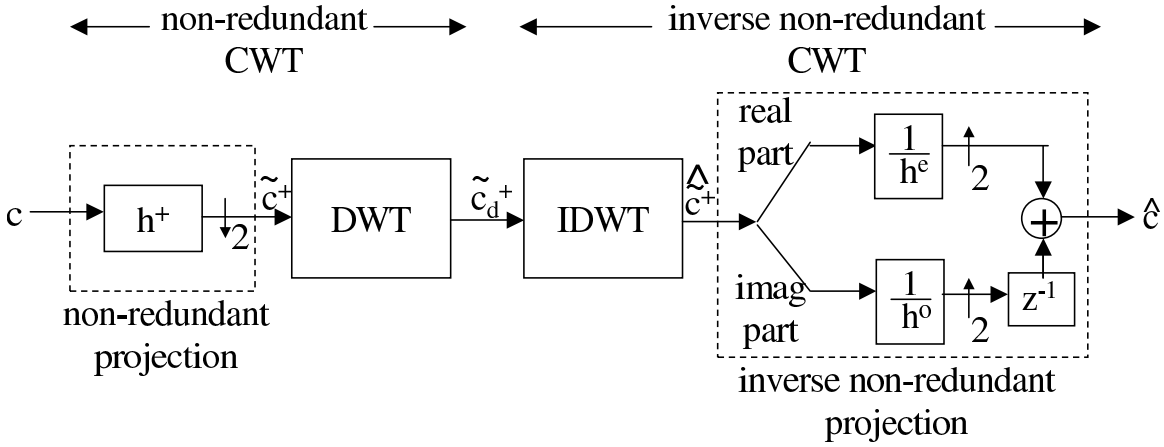

Figure 5: Filter-bank implementation of the Non-Redundant CWT and its Inverse. The symbols $\frac{1}{h^e}, \frac{1}{h^o}$ represent the filters $\frac{1}{H^e(-z)}, \frac{1}{H^o(-z)}$ respectively.

Now that we have defined the non-redundant projection and examined its properties, we are ready to introduce the non-redundant CWT. We refer the reader to Figure 5. The scaling coefficient sequence c undergoes a non-redundant projection that outputs $\widetilde{c}^+$. The DWT of $\widetilde{c}^+$ is $\widetilde{c}^+_d$ the non-redundant CWT of c. In [7], we demonstrate that the non-redundant CWT is an orthogonal transform if it uses an orthogonal DWT along with a projection filter h^+ that is created by modulating a lowpass filter having allpass polyphase components. Specifically, $H^+(z) = H^0(-jz)$ where $H^0(z) = H^e(z^2) + z^{-1}H^o(z^2)$, and $H^e(z), H^o(z)$ are allpass filters selected to create the lowpass filter h^0. Thus orthogonality places a design constraint on the projection filter h^+.

To invert the non-redundant CWT, we first compute $\widehat{\widetilde{c}^+}$, the inverse DWT of $\widetilde{c}^+_d$. Finally, we must invert the non-redundant projection. In [7], we prove that the block labeled "inverse non-redundant projection" in Fig. 5 operates on $\widehat{\widetilde{c}^+}$ to invert the non-redundant projection. This

block separates the real and imaginary components of $\widehat{\widetilde{c}^+}$ and passes them through filters $1/H^e(-z)$ and $1/H^o(-z)$ respectively. Note that these are allpass filters because $H^e(z)$ and $H^o(z)$ are the allpass polyphase components of $H^0(z)$. The outputs of $1/H^e(-z)$ and $1/H^o(-z)$ are the polyphase components of the reconstructed scaling coefficient sequence $\hat{c}$.

3.2.3 Designing the Projection Filter

As seen above, orthogonality places a design constraint on h^0 the lowpass filter that is modulated to generate h^+. Another design constraint that becomes evident in Section 3.4 is that $H^0(z)$ must be a root-halfband filter so that $H^0(z)H^0(z^{-1}) + H^0(-z)H^0(-z^{-1}) = 1$. The design of lowpass filters satisfying these two constraints has been reported previously [30, 39, 34]. In this paper, we shall use these reported techniques to generate two different projection filters and then compare the non-redundant CWTs that use these filters. The first projection filter $h^+_{maxflat}$ is created by modulating a maximally flat, allpass-sum, lowpass filter designed by Selesnick [39]. The second projection filter $h^+_{minimax}$ is generated by modulating the minimax, allpass-sum, lowpass filter described in Schuessler and Steffen's article [34].

The first maximally flat projection filter is given by

$$H^+_{maxflat}(z) = H^0_{maxflat}(-jz), \tag{2}$$

where

$$H^0_{maxflat}(z) = H^e_{maxflat}(z^2) + z^{-1}H^o_{maxflat}(z^2),$$

and $H^e_{maxflat}(z), H^o_{maxflat}(z)$ are allpass polyphase components of $H^0_{maxflat}(z)$ given by

$$\begin{aligned} H^e_{maxflat}(z) &= \frac{0.1056 + z^{-1}}{1 + 0.1056z^{-1}}, \\ H^o_{maxflat}(z) &= \frac{0.5279 + z^{-1}}{1 + 0.5279z^{-1}}. \end{aligned}$$

Similarly, for the minimax projection filter, we have

$$H^+_{minimax}(z) = H^0_{minimax}(-jz), \tag{3}$$

where

$$H^0_{minimax}(z) = H^e_{minimax}(z^2) + z^{-1}H^o_{minimax}(z^2),$$

and $H^e_{minimax}(z), H^o_{minimax}(z)$ are allpass polyphase components of $H^0_{minimax}(z)$ given by

$$\begin{aligned} H^e_{minimax}(z) &= \frac{0.1874 + z^{-1}}{1 + 0.1874z^{-1}}, \\ H^o_{minimax}(z) &= \frac{0.6562 + z^{-1}}{1 + 0.6562z^{-1}}. \end{aligned}$$

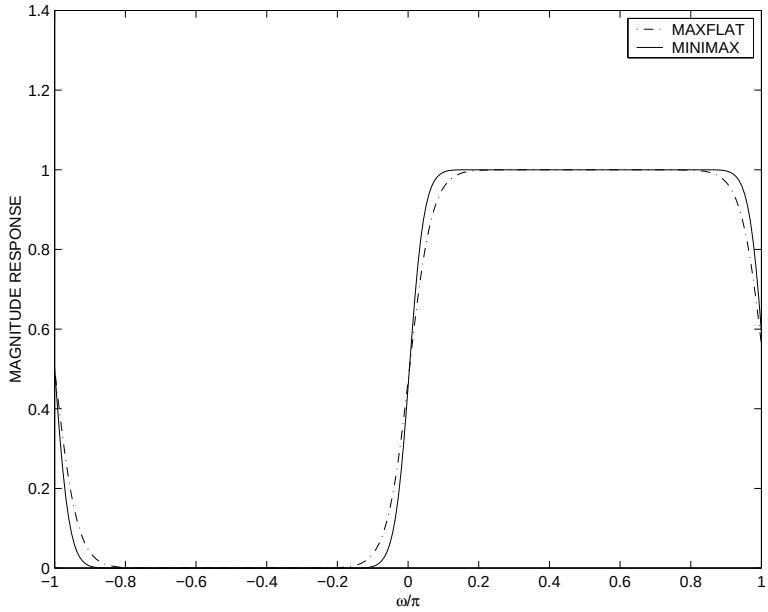

Figure 6: Magnitude Responses of Minimax and Maximally Flat Projection Filters

Figure 6 compares the magnitude responses of the minimax and maximally flat projection filters. Observe that the transition band of the minimax projection filter is sharper than that of the maximally flat projection filter, although both filters have equal computational complexity. In Section 3.5, we shall demonstrate that a two-dimensional non-redundant CWT using the minimax projection filter has better directionality than a comparable non-redundant CWT with a maximally flat projection filter. In the next section, we motivate the two dimensional (2D) extension of the non-redundant CWT by discussing the poor directionality of the 2D RWT.

3.3 Poor Directionality in the RWT

The separable two-dimensional (2D) RWT is a powerful image-processing tool, but in some applications its poor directionality is a serious disadvantage because the 2D RWT can distinguish between only three different orientations of spatial features: horizontal, vertical and diagonal. In Fig. 7, we illustrate the poor directionality of the RWT. Fig. 7(a) shows an image of a disc to which we apply a level-one RWT and obtain the *HL*, *LH*, *HH* subbands shown in Figs. 7(b), (c), (d). Observe that the RWT subbands differentiate between only *three* feature-orientations: horizontal, vertical and diagonal features. In this section, we explain the poor directionality of the 2D RWT based on the Fourier-plane tiling associated with its subbands. In the next section, we introduce the two-dimensional extension of the non-redundant CWT. The Fourier-plane partitioning of this

(a) (b) (c) (d)

Figure 7: (a) Disc Image, (b) RWT HL subband: Vertical edges, (c) RWT LH subband: Horizontal edges, (d) RWT HH subband: Diagonal edges

transform is responsible for the improvement in directionality: it enables distinctions between *six* spatial feature-orientations at $+15, +45, +75, -75, -45, -15$ degrees.

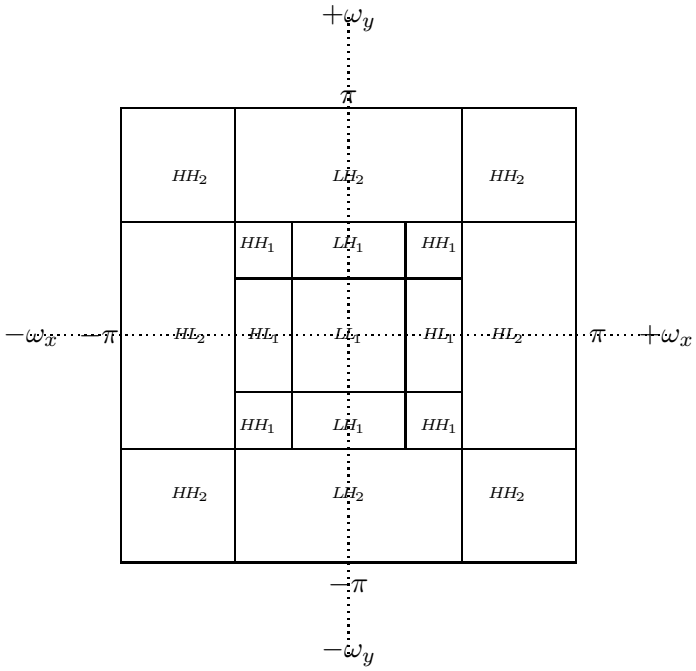

Figure 8: Fourier-plane partitioning obtained from a separable two-level 2D RWT.

Figure 8 shows the Fourier-plane partitioning obtained from a separable, two-level 2D RWT. The HH_2 subband is associated with diagonally-oriented spatial features at scale 2 and concentrates its energy in the four blocks labeled HH_2. High energy at the output of the filter in the HH_2 subband indicates the presence of this class of features. The HH_2 blocks in the upper-left and lower-right corners indicate features whose gradients are oriented at -45 degrees, while those in the upper-right and lower-left corners indicate feature-gradient orientations of $+45$ degrees [13]. Since all four blocks are associated with the output of a single filter in the RWT, we cannot differentiate between these two orientations. Similarly, feature-gradient orientations at $+15$ degrees and -15 degrees are

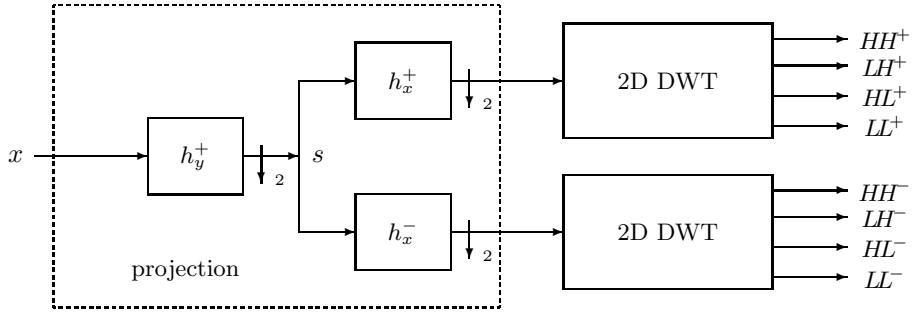

Figure 9: The non-redundant 2D CWT

indistinguishable from their wavelet coefficients since they are both associated with energy in the HL_2 subband. Features with gradients oriented at $+75$ degrees and -75 degrees suffer a similar fate. It is evident that the poor directionality of the RWT is due to positively- and negatively-oriented blocks both being associated with the same subband. In the following section, we introduce the two-dimensional non-redundant projection that will decouple these blocks, thereby improving directionality.

3.4 Improving directionality with the 2D non-redundant CWT

In Section 3.2 we defined the non-redundant CWT, a wavelet transform that offers phase information without incurring any data redundancy. We shall now extend this transform to two dimensions so that it may be applied to images. This will provide improved directionality without any additional redundancy.

Fig. 9 illustrates the two-dimensional extension of the non-redundant CWT. In [7, Pg. 73], we argue that for signals with a lowpass frequency-domain characteristic, the frequency-domain action of the non-redundant projection is similar to that of the redundant projection. Therefore, while discussing the directionality of the non-redundant CWT we shall ignore the downsamplers in Fig. 9. To explain the 2D non-redundant CWT, we shall first extend the non-redundant projection to two dimensions. Next, we shall describe how 2D DWTs are applied to the projection to obtain the 2D non-redundant CWT.

3.4.1 The 2D Non-Redundant Projection

A one-dimensional $L^2(\mathbb{R} \to \mathbb{R})$ function is fully described by its positive frequencies in the Fourier domain. Since the negative frequencies carry redundant information they may be zeroed out thereby

yielding the Hardy-space image of the function. Similarly, for real-valued two-dimensional images, the lower half-plane of the Fourier transform carries redundant information. We may eliminate this redundant information to obtain a complex-valued spatial image with phase information by filtering the columns of the image with a projection filter h_y^+ as shown in Fig. 9. The subscript "y" indicates that the projection filter h^+ is applied along the image columns.

To eliminate the redundant information contained in the negative vertical frequencies, we use the projection filter h_y^+ to project the image columns onto an approximation to the Hardy space. In one dimension, elimination of redundant information along the negative half-line of the Fourier plane provides phase information. However, eliminating the negative vertical half-plane in the two-dimensional Fourier plane and then performing the DWT does not improve DWT directionality. To do so, we must decouple the positive, horizontal frequencies from the negative, horizontal frequencies.

We show how this may be done in Figure 9. The h_y^+ projection filter retains the positive vertical frequencies. The h_x^+ filter is a projection filter that operates along the rows of the h_y^+ filter's output and retains the positive horizontal frequencies. Therefore the output from the h_x^+ filter is associated with the block labeled "h_x^+ output" in Fig. 10. This block contains the positive-vertical, positive-horizontal frequencies.

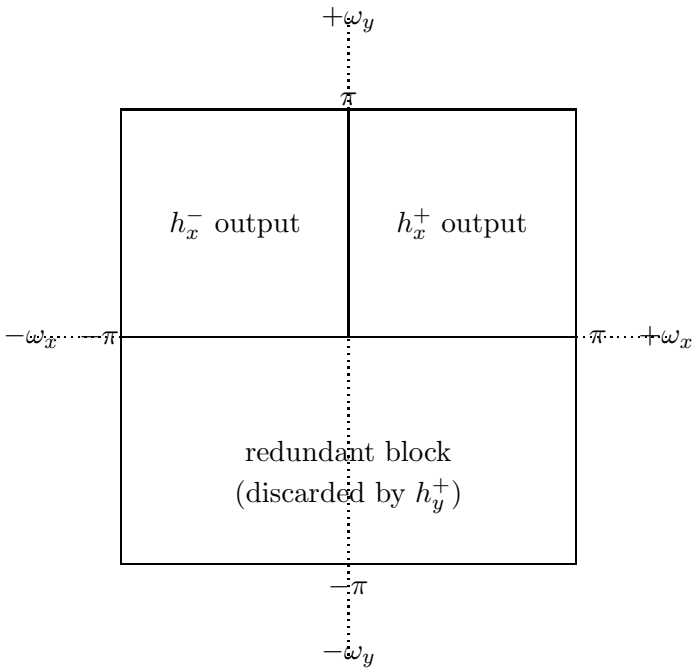

Figure 10: Fourier-plane partitioning after 2D Softy-space projection.

Recall that the h_x^+ projection filter retains positive frequencies and suppresses negative frequen-

cies. The h_x^- projection filter performs a similar operation: it retains negative horizontal frequencies and suppresses positive horizontal frequencies. The output from this filter is associated with the block labeled "h_x^- output" in Fig. 10. This block contains the positive-vertical, negative-horizontal frequencies. Therefore the "projection" module in Fig. 9 eliminates the redundant negative-vertical frequencies and decouples the positive horizontal frequencies from the negative horizontal frequencies, as is evident in Fig. 10.

3.4.2 The 2D Non-Redundant CWT and its Inverse

Having defined the 2D extension of the Softy-space projection, we are ready to define the 2D non-redundant CWT. This is easily done by performing 2D DWTs on the images output by the "projection" module in Fig. 9. Applying a 2D two-level DWT to the output of the h_x^+ filter partitions the " h_x^+ output" block of Fig. 10 into the subbands with the "+" superscripts in Fig. 11. Similarly the 2D two-level DWT applied to the h_x^- filter output yields the subbands with the "-" superscripts in Fig. 11. The decoupled $HL^+, HH^+, LH^+, LH^-, HH^-, HL^-$ subbands provide the 2D non-redundant CWT with better directionality than the RWT. We shall examine the directionality of these subbands in Section 3.5. Now we shall describe the inverse 2D non-redundant CWT.

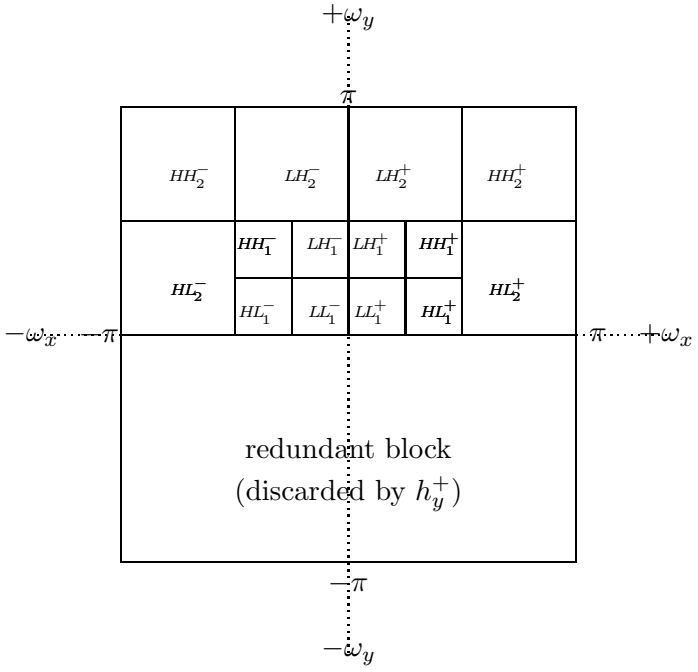

Figure 11: Fourier-plane partitioning of the 2D two-level CWT.

To invert the non-redundant 2D CWT, we propose the structure shown in Fig. 12. The blocks labeled "2D IDWT" invert the 2D DWTs that were applied to the decoupled images. Next we must

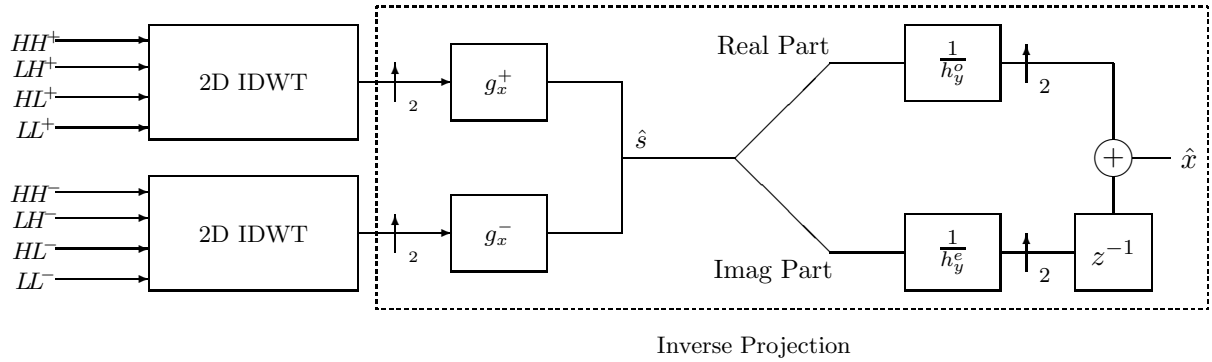

Figure 12: The non-redundant 2D ICWT. The symbols $\frac{1}{h_y^e}, \frac{1}{h_y^o}$ represent the filters $\frac{1}{H^e(-z)}, \frac{1}{H^o(-z)}$ operating along the image columns.

invert the non-redundant projections applied along the image rows. Recall that the projection filter h^+ is a root-halfband filter. This design constraint allows h_x^+ and h_x^- to constitute the analysis bank of a 2-band decimated filter bank [47, 45]. Therefore the corresponding synthesis filter bank comprised of filters g^+ and g^- will invert this analysis filter bank and output $\hat{s}$. As explained in Section 3.2.2 the filters $1/H^e(-z), 1/H^o(-z)$ operate on the real and imaginary parts of rows in $\hat{s}$ to invert the non-redundant projection operation performed by h_x^+ followed by a downsampler. Finally, we recombine the polyphase outputs of the filters $1/H^e(-z), 1/H^o(-z)$ and obtain $\hat{x}$, the reconstructed image. In the next section, we explain the improved directionality of the non-redundant 2D CWT.

3.5 Directionality of the 2D Non-redundant CWT

The 2D non-redundant CWT has improved directionality because, at each scale, it provides the six directional subbands $HL^+, HH^+, LH^+, LH^-, HH^-, HL^-$ shown in Fig. 11. As explained in Section 3.4, these decoupled subbands describe feature-gradients oriented at $+15, +45, +75, -75, -45, -15$ degrees, respectively. We illustrate this improved directionality in Fig. 13(a)–(f) where we show the directional, level-one subbands of the 2D non-redundant CWT applied to the disc image in Fig. 7(a). On comparing to the RWT disc-decomposition in Fig. 13(b)–(d), it is clear that the directionality of the 2D CWT is significantly better than that of the 2D RWT which has only three directional subbands: horizontal, vertical and diagonal.

We created the 2D non-redundant CWT decomposition in Figs. 13 (a)–(f) by using the maximally flat projection filter $h_{maxflat}^+$ described in Equation 2. However, the directionality of the decomposition is improved slightly if the minimax projection filter of Equation 3 is used instead. The

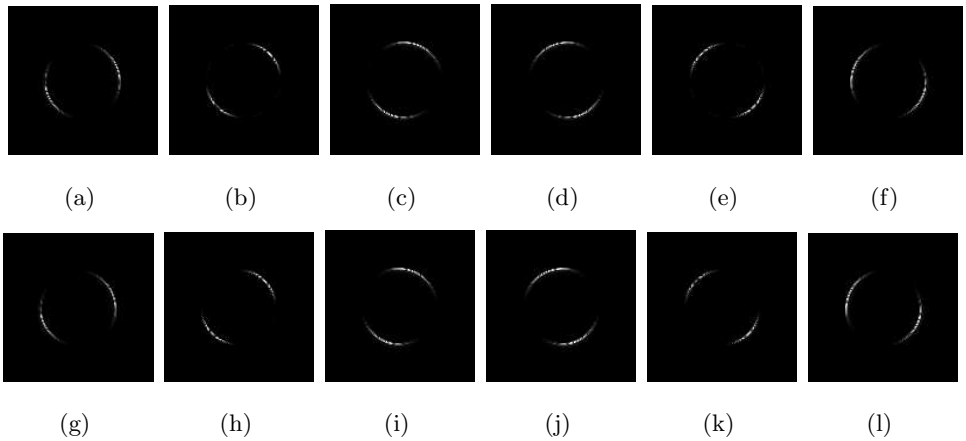

Figure 13: (a) $HL^{+}_{maxflat}$ subband: $+15^\circ$ feature-gradients, (b) $HH^{+}_{maxflat}$ subband: $+45^\circ$ feature-gradients, (c) $LH^{+}_{maxflat}$ subband: $+75^\circ$ feature-gradients, (d) $LH^{-}_{maxflat}$ subband: -75° feature-gradients, (e) $HH^{-}_{maxflat}$ subband: -45° feature-gradients, (f) $HL^{-}_{maxflat}$ subband: -15° feature-gradients, (g) $HL^{+}_{minimax}$ subband: $+15^\circ$ feature-gradients, (h) $HH^{+}_{minimax}$ subband: $+45^\circ$ feature-gradients, (i) $LH^{+}_{minimax}$ subband: $+75^\circ$ feature-gradients, (j) $LH^{-}_{minimax}$ subband: -75° feature-gradients, (k) $HH^{-}_{minimax}$ subband: -45° feature-gradients, (l) $HL^{-}_{minimax}$ subband: -15° feature-gradients.

directional subbands obtained from the decomposition with this filter are shown in Figs. 13(g)–(l). The improvement in directional selectivity is evident from a comparison of corresponding subbands in the two decompositions. For example, Figs. 13(e) and (k) show the HH^{-} subbands from the non-redundant CWT using maximally flat and minimax projection filters respectively. Recall that the HH^{-} subband reveals feature-gradient orientations at -45 degrees. Therefore, the upper-right and lower-left quadrants of the HH^{-} subbands should be dark because the input disc image has $+45$ degree feature-gradient orientations in these locations. Careful examination of Figs. 13(e) and (k) shows that these quadrants are indeed darker in Fig. 13(k) than in Fig. 13(e). To make the comparison easier, we placed the upper-right quadrant of Fig. 13(e) in the upper half of Fig. 14 and the upper-right quadrant of Fig. 13(k) in the lower half of Fig 14. Clearly, the upper-right quadrant of Fig. 13(k) is suppressed to a greater extent than the upper-right quadrant of Fig. 13(e). Therefore, we conclude that the minimax projection filter provides a 2D non-redundant CWT decomposition with better directional selectivity than that obtained using a maximally flat projection filter with the same computational complexity.

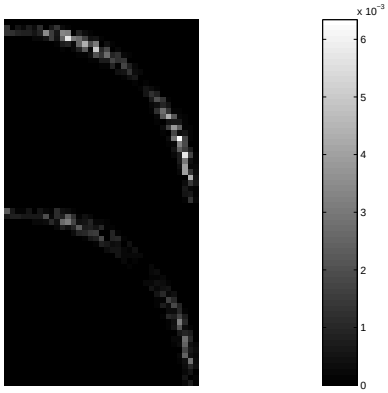

Figure 14: The upper half of the figure shows the upper-right quadrant of the HH^- subband from the 2D non-redundant CWT using a maximally flat projection filter. The lower half of the figure shows the corresponding quadrant from a 2D non-redundant CWT with a minimax projection filter.

4 Dual-Tree Complex Wavelet Transform

Let the real filters $h_0(n)$, $h_1(n)$ represent a conjugate quadrature filter (CQF) pair [44]. That is, the autocorrelation of the lowpass filter $h_0(n)$ is halfband:

$$p_h(2\,n) = \delta(n) = \begin{cases} 1, & n = 0 \\ 0, & n \neq 0, \end{cases} \tag{4}$$

where

$$p_h(n) := h_0(n) * h_0(-n)$$

and the highpass filter is given by: $h_1(n) = (-1)^n\, h_0(M-n)$ where M is an odd integer. Let the real filters $g_0(n)$, $g_1(n)$ represent a second CQF pair. The real-valued scaling function $\phi_h(t)$ and the real-valued wavelet $\psi_h(t)$ associated with the pair $(h_0(n), h_1(n))$ are defined implicitly by the following pair of equations:

$$\phi_h(t) = \sqrt{2} \sum_n h_0(n)\, \phi_h(2t-n) \tag{5}$$

$$\psi_h(t) = \sqrt{2} \sum_n h_1(n)\, \phi_h(2t-n). \tag{6}$$

The real-valued scaling function $\phi_g(t)$ and wavelet $\psi_g(t)$ associated with the pair $(g_0(n), g_1(n))$ are defined similarly.

Notation: The Z-transform of $h(n)$ is denoted by $H(z)$. The discrete-time Fourier transform of

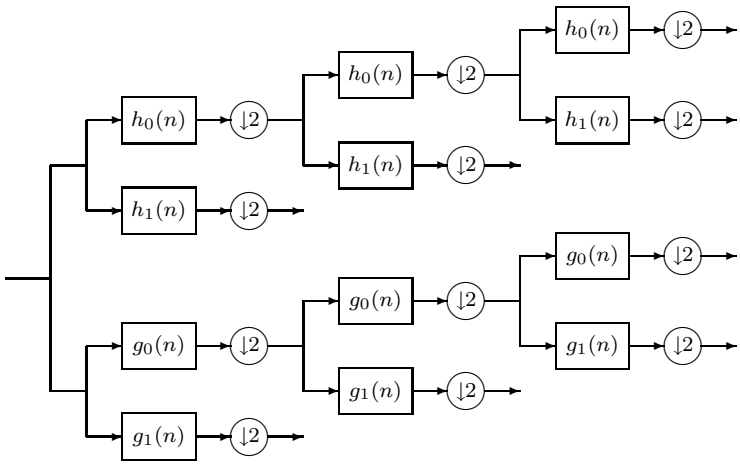

Figure 15: The 1-D dual-tree wavelet transform is implemented using a pair of filter banks operating on the same data simultaneously. The upper iterated filter bank represents the real part of a complex wavelet transform, the lower one represents the imaginary part. The transform is an expansive (or oversampled) transform (or *frame*).

$h(n)$ will be denoted by $H(e^{j\omega})$,

$$H(e^{j\omega}) = \sum_n h(n)\, e^{-j\, n\, \omega}.$$

The Fourier transform of $\psi(t)$ is denoted by $\Psi(\omega) = \mathcal{F}\{\psi(t)\}$.

4.1 Hilbert Pairs

To implement a complex wavelet transform, Kingsbury suggested using two independent wavelet transforms operating in parallel on the same data. Then a complex-valued wavelet $\psi(t)$ can be obtained as

$$\psi(t) = \psi_h(t) + j\, \psi_g(t)$$

where $\psi_h(t)$ and $\psi_g(t)$ are both real-valued wavelets. Note that a complex transform implemented in this way is not critically-sampled because two independent wavelet transforms are required.

The benefits of complex wavelet transforms depend on the spectrum of the complex-valued wavelet $\psi(t)$ being single sided ($\Psi(\omega) = 0$ for $\omega \leq 0$). To have this property, it is required that the wavelet $\psi_g(t)$ be the Hilbert transform of the wavelet $\psi_h(t)$. Specifically,

$$\Psi_g(\omega) = \begin{cases} -j\ \Psi_h(\omega), & \omega > 0 \\ \ \ j\ \Psi_h(\omega), & \omega < 0 \end{cases}$$

which we denote as

$$\psi_g(t) = \mathcal{H}\{\psi_h(t)\}. \tag{7}$$

One question which arises is, how should the two lowpass filters $h_0(n)$ and $g_0(n)$ satisfying the CQF properties above be designed so that the corresponding wavelets form a Hilbert pair? The wavelets are defined only implicitly through the equations (5,6), but using the infinite product formula it was shown in [40] how the two lowpass filters can be chosen. Namely, it was shown that if $H_0(\omega)$ and $G_0(\omega)$ are lowpass filters with

$$G_0(\omega) = H_0(\omega)\, e^{-j\,0.5\,\omega} \quad \text{for} \quad |\omega| < \pi, \tag{8}$$

then the wavelets corresponding to these filters form a Hilbert transform pair. Informally, if in the time-domain we have $g_0(n) = h_0(n-0.5)$, then $\psi_g(t) = \mathcal{H}\{\psi_h(t)\}$. If it is desired that both lowpass filters $h_0(n)$ and $g_0(n)$ be FIR, then it is impossible to satisfy (8) exactly and an approximation must be made.

The widely used wavelets constructed by Daubechies are based on CQF filters the transfer functions of which have a specified number of zeros at $z = -1$. The delay condition (8) is an additional constraint which must be included into the design of filters $h_0(n)$ and $g_0(n)$. In [41], the Daubechies construction is modified so that the delay condition (8) can be included. With this modification, pairs of compactly supported wavelets with vanishing moments can be obtained that approximately satisfy the Hilbert property (7).

The construction described in [41] requires an allpass system $A(z)$ which approximates a half sample delay, and it is suggested that a maximally flat delay allpass system be used. However, any allpass system with an approximately constant delay of a half sample can be used. The better the allpass system approximates the constant delay of a half sample, the closer the resulting pair of wavelets will be to a Hilbert transform pair. In particular, an allpass system designed according to the minimax (Chebyshev) criterion can be used. The examples presented here will show that using allpass systems of this type yields pairs of wavelets which more closely satisfy the condition (7). Consequently, the spectrum $\Psi(\omega)$ of the complex-valued wavelet $\psi(t)$ will more accurately approximate zero for $\omega < 0$.

4.2 Orthogonal Solutions

To obtain a pair of lowpass filters $h_0(n)$, $g_0(n)$ satisfying the CQF condition (4) and the delay condition (8), it was proposed in [41] that they have the following form:

$$H_0(z) = F(z)\, D(z) \tag{9}$$

$$G_0(z) = F(z)\, z^{-L}\, D(1/z). \tag{10}$$

By appropriately designing the transfer function $D(z)$ of degree L, the delay condition (8) can be approximately satisfied. $H_0(z)$ and $G_0(z)$ have $F(z)$ in common, which will be determined below. From (9, 10) we have

$$G_0(z) = H_0(z)\, \frac{z^{-L}\, D(1/z)}{D(z)}$$

where we can recognize the transfer function

$$A(z) := \frac{z^{-L}\, D(1/z)}{D(z)}$$

is an allpass system, $|A(e^{j\omega})| = 1$. Therefore $|G_0(e^{j\omega})| = |H_0(e^{j\omega})|$, $|G_1(e^{j\omega})| = |H_1(e^{j\omega})|$, and by the infinite-product formula $|\Psi_g(\omega)| = |\Psi_h(\omega)|$. If the allpass system $A(z)$ is an approximate half-sample delay, $A(e^{j\omega}) \approx e^{-j\,0.5\,\omega}$, then the delay condition (8) is approximately satisfied: $G_0(e^{j\omega}) \approx H_0(e^{j\omega}) e^{-j\,0.5\,\omega}$. Note that because it is not practical to ask that $A(e^{j\omega}) \approx e^{-j\,0.5\,\omega}$ for all $|\omega| < \pi$, it is necessary to specify some band over which the this approximation is accurate. Since $G_0(e^{j\omega})$ and $H_0(e^{j\omega})$ are lowpass filters, we will ask of the allpass system that $A(e^{j\omega}) \approx e^{-j\,0.5\,\omega}$ for $|\omega| < 0.5\,\pi$.

We therefore propose designing $D(z)$ by designing an allpass system $A(z)$ according to the minimax criterion. The desired phase of $A(z)$ is $-0.5\,\omega$. The design of $A(z)$ so as to minimize

$$\max_{|\omega| \le 0.5\,\pi} |\text{phase of} A(z) + 0.5\,\omega|$$

can be performed using the allpass approximation algorithms referenced in Section 2.

We will ask of $H_0(z)$ and $G_0(z)$ that they have K zeros at $z = 1$ and in addition zeros at $z = e^{\pm\, j\,\omega_o}$. This additional null in the stop-band of the lowpass filter can improve the flexibility of the design procedure. The two lowpass filters then have the following form:

$$H_0(z) = Q(z)\, (1 + z^{-1})^K\, (1 + 2\, \cos(\omega_o)\, z^{-1} + z^{-2})\, D(z), \tag{11}$$

$$G_0(z) = Q(z)\, (1 + z^{-1})^K\, (1 + 2\, \cos(\omega_o)\, z^{-1} + z^{-2})\, z^{-L}\, D(1/z). \tag{12}$$

The problem now is to find $Q(z)$ so that $h_0(n)$ and $g_0(n)$ satisfy the CQF conditions (4). Because $h_0(n)$ and $g_0(n)$ have the same autocorrelation function:

$$P(z) := P_h(z) = P_g(z) \tag{13}$$

$$= Q(z)\,Q(1/z)\,(z+2+z^{-1})^K\,(z+2\,\cos(\omega_o)+z^{-1})^2\,D(z)\,D(1/z). \tag{14}$$

we can follow Daubechies construction to obtain $Q(z)$ using a spectral factorization approach as in [44]:

1. Find a symmetric sequence $r(n)$ of minimal length $[r(n) = r(-n)]$ such that

   $$V(z) = R(z)\,(z+2+z^{-1})^K\,(z+2\,\cos(\omega_o)+z^{-1})^2\,D(z)\,D(1/z)$$

   is the transfer function of a halfband filter. That is, $v(2\,n) = \delta(n)$.

   The sequence $r(n)$ can be obtained by solving a square system of linear equations. Setting

   $$S(z) := (z+2+z^{-1})^K\,(z+2\,\cos(\omega_o)+z^{-1})^2\,D(z)\,D(1/z)$$

   we can write the halfband condition as

   $$\delta(n) = [\downarrow 2]\,(s * r)(n) \tag{15}$$

   $$= \sum_k s(2n-k)\,r(k). \tag{16}$$

   In matrix form, we have a square matrix which has the form of a convolution (Toeplitz) matrix with every second row deleted.

2. Set $Q(z)$ to be a spectral factor of $R(z)$,

   $$R(z) = Q(z)\,Q(1/z). \tag{17}$$

   Because $Q(z)$ is given by spectral factorization, it is not unique. Like Daubechies construction, there are different solutions with varying degree of symmetry. We have assumed here that spectral factorization is possible. In [12] Gopinath has proven that when $D(z)$ is a maximally-flat delay polynomial (and the stopband null ω_o is absent) then spectral factorization is always possible. We have found that when the minimax criterion is used to design $D(z)$ then in our examples the spectral factorization of $R(z)$ has also been possible.

Example: With $K = 2$, $L = 2$, and $\omega_o = 0.8\,\pi$ the filters $h_0(n)$ and $g_0(n)$ are of length 12. The magnitude of the frequency response $|H_0(e^{j\,\omega})|$ and the zeros of $H_0(z)$ are shown in Figure 16. We

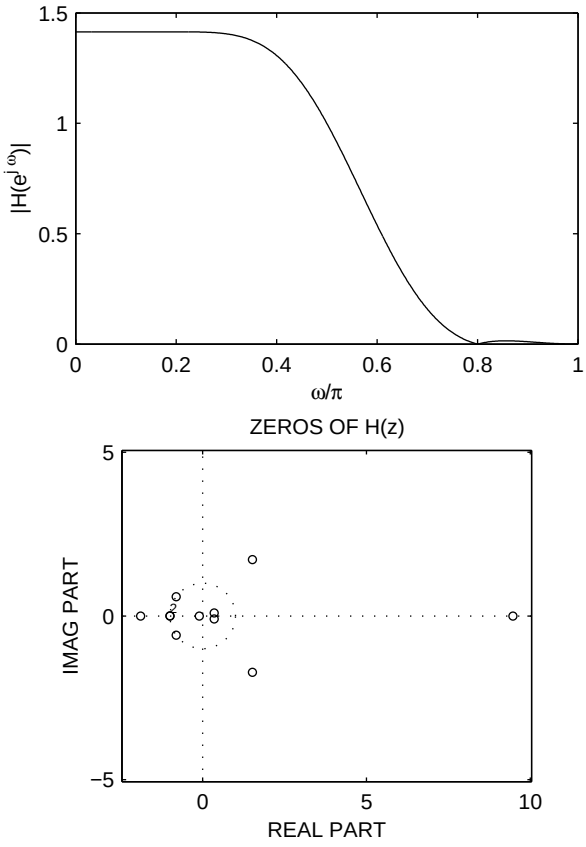

Figure 16: Frequency response of $h_0(n)$

used in (17) a mid-phase spectral factorization to make the wavelets more symmetric than they would be otherwise. The wavelets $\psi_h(t)$ and $\psi_g(t)$ are shown in Figure 17. The figure also shows the magnitude of the complex wavelet $|\psi(t)|$ where $\psi(t) = \psi_h(t) + j\,\psi_g(t)$. The envelope, shown as a dashed line, does not have the oscillatory behavior the wavelets themselves have. In the second panel of the figure, the magnitude of the spectrum of the complex wavelet, $|\Psi(\omega)|$, is also shown. Note that $\Psi(\omega) \approx 0$ for $\omega < 0$ which verifies that the two wavelets form an approximate Hilbert pair. The third panel of the figure shows a magnification of $|\Psi(\omega)|$. The dashed line shows $|\Psi(\omega)|$ when a maximally-flat delay polynomial $D(z)$ of degree 2 is used in the design procedure. It can be seen that when the maximally-flat polynomial is used, instead of one designed according to the minimax criterion, the approximation suffers. With the minimax type, $|\Psi(\omega)|$ approximates zero for negative frequencies with substantial improvement — the error is reduced by over a factor of two.

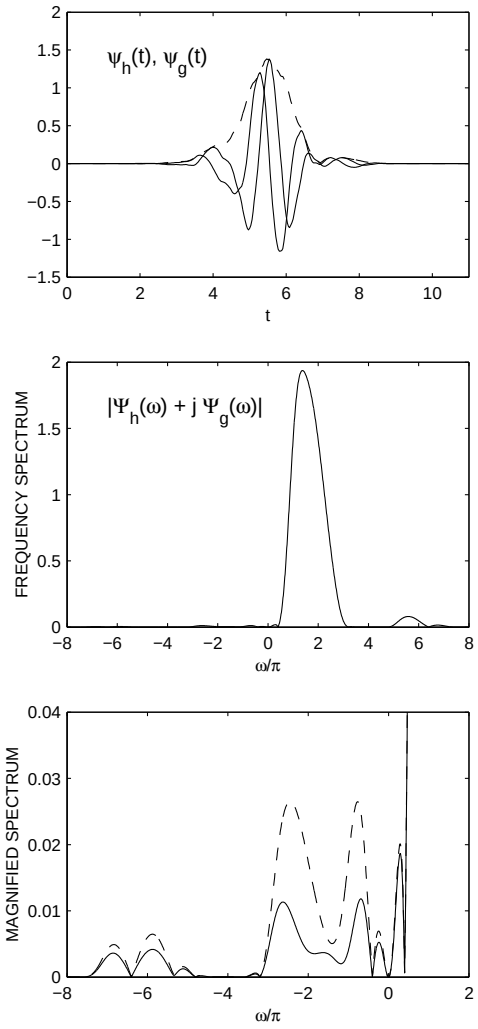

Figure 17: A pair of wavelets which form an approximate Hilbert pair. The complex wavelet $\psi(t) = \psi_h(t) + j\,\psi_g(t)$ has a spectrum $\Psi(\omega)$ which is approximately single sided. The dashed curve in the lower panel illustrates the solution corresponding to a design based on the maximally-flat delay allpass system. The solution obtained with a minimax delay allpass system approximates more accurately the Hilbert pair property.

4.3 Biorthogonal Dual-Tree

In the biorthogonal case, we have the dual scaling functions and wavelets by $\widetilde{\phi}_h(t)$, $\widetilde{\psi}_h(t)$, $\widetilde{\phi}_g(t)$, and $\widetilde{\psi}_g(t)$. With the biorthogonal solution, the complex wavelet $\psi(t) = \psi_h(t) + j\,\psi_g(t)$ will have a symmetric magnitude: $|\psi(-t)| = |\psi(t)|$, as will the dual complex wavelet $\widetilde{\psi}(t) = \widetilde{\psi}_h(t) + j\,\widetilde{\psi}_g(t)$.

The dual scaling function $\widetilde{\phi}_h(t)$ and wavelet $\widetilde{\psi}_h(t)$ are given by the equations,

$$\widetilde{\phi}_h(t) = \sqrt{2} \sum_n \widetilde{h}_0(n)\, \widetilde{\phi}_h(2t - n) \tag{18}$$

$$\widetilde{\psi}_h(t) = \sqrt{2} \sum_n \widetilde{h}_1(n)\, \widetilde{\phi}_h(2t - n). \tag{19}$$

The dual scaling function $\widetilde{\phi}_g$ and wavelet $\widetilde{\psi}_g$ are similarly defined.

The goal will be to design the filters so that both the primary (synthesis) and dual (analysis) wavelets form approximate Hilbert transform pairs,

$$\psi_g(t) = \mathcal{H}\{\psi_h(t)\} \quad \text{and} \quad \widetilde{\psi}_g(t) = \mathcal{H}\{\widetilde{\psi}_h(t)\}.$$

If we define the product filters as

$$p_h(n) := \widetilde{h}_0(n) * h_0(n) \tag{20}$$

$$p_g(n) := \widetilde{g}_0(n) * g_0(n), \tag{21}$$

then the biorthogonality conditions can be written as

$$p_h(2n + n_o) = \delta(n) \tag{22}$$

$$p_g(2n + n_o) = \delta(n). \tag{23}$$

That is to say, p_h, p_g must both be halfband. Without loss of generality, we can assume that n_o is an odd integer. In that case, the highpass filters are given by the following expressions [5, 47].

$$h_1(n) := (-1)^n\, \widetilde{h}_0(n) \tag{24}$$

$$\widetilde{h}_1(n) := -(-1)^n\, h_0(n) \tag{25}$$

$$g_1(n) := (-1)^n\, \widetilde{g}_0(n) \tag{26}$$

$$\widetilde{g}_1(n) := -(-1)^n\, g_0(n) \tag{27}$$

We will look for solutions of the form

$$h_0(n) = f(n) * d(n) \tag{28}$$

$$\widetilde{h}_0(n) = \widetilde{f}(n) * d(L-n) \tag{29}$$

$$g_0(n) = f(n) * d(L-n) \tag{30}$$

$$\widetilde{g}_0(n) = \widetilde{f}(n) * d(n). \tag{31}$$

The problem is to find $f(n)$ and $\widetilde{f}(n)$ such that (i) the biorthogonality conditions (22,23) are satisfied, (ii) the wavelets have K vanishing moments ($\widetilde{K}$ vanishing moments for the dual wavelets), and in addition zeros at $z = e^{\pm j\,\omega_o}$. and (iii) the wavelets form an approximate Hilbert transform pair.

To obtain the half sample delay, needed to ensure the approximate Hilbert property, we choose $d(n)$ to come from an allpass filter as before,

$$A(z) = \frac{z^{-L}\,D(1/z)}{D(z)} \approx z^{-1/2} \quad \text{around } z = 1.$$

To ensure the vanishing moments properties, we take $F(z)$ and $\widetilde{F}(z)$ to be of the form,

$$F(z) = Q(z)\,(1+z^{-1})^K\,(1+2\,\cos(\omega_o)\,z^{-1}+z^{-2}) \tag{32}$$

$$\widetilde{F}(z) = \widetilde{Q}(z)\,(1+z^{-1})^{\widetilde{K}}\,(1+2\,\cos(\omega_o)\,z^{-1}+z^{-2}) \tag{33}$$

where $K+\widetilde{K}$ is odd. K denotes the number of vanishing moments of the primary (synthesis) wavelets, and $\widetilde{K}$ denotes the number of vanishing moments of the dual (analysis) wavelets. The product filters p_h and p_g are then given by

$$P(z) := P_h(z) = P_g(z) \tag{34}$$

$$= Q(z)\,\widetilde{Q}(z)\,(1+z^{-1})^{K+\widetilde{K}}\,(z+2\,\cos(\omega_o)+z^{-1})^2\,D(z)\,D(1/z)\,z^{-L}. \tag{35}$$

To obtain the required halfband property, we find a symmetric odd-length sequence $r(n)$ so that

$$R(z)\,(1+z^{-1})^{K+\widetilde{K}}\,(z+2\,\cos(\omega_o)+z^{-1})^2\,D(z)\,D(1/z)\,z^{-L}$$

is halfband. The symmetric sequence $r(n)$ can be obtained by solving a linear system of equations as in Section 4.2. We can then obtain $Q(z)$ and $\widetilde{Q}(z)$ by factoring $R(z)$,

$$R(z) = Q(z)\,\widetilde{Q}(z), \tag{36}$$

where both $q(n)$ and $\widetilde{q}(n)$ are symmetric. As $q(n)$ and $\widetilde{q}(n)$ are symmetric, so are $f(n)$ and $\widetilde{f}(n)$. It follows that $h_0(n)$ and $g_0(n)$ are related by a reversal, $g_0(n) = h_0(N-1-n)$, and similarly,

$\widetilde{g}_0(n) = \widetilde{h}_0(N-1-n)$. Therefore, h_0, $\widetilde{h}_0$, g_0 and $\widetilde{g}_0$ have approximately linear phase (because $d(n)$ does) in addition to satisfying the condition (8) approximately. Note that the symmetric factorization (36) is not unique — many solutions are available. Also note that the sequences $f(n)$ and $\widetilde{f}(n)$ do not need to have the same length.

Example: With $K = \widetilde{K} = 2$, $L = 2$, and $\omega_o = 0.8\,\pi$ we can take the synthesis filters $h_0(n)$ and $g_0(n)$ to be of length $N = 13$. The analysis filters $\widetilde{h}_0(n)$ and $\widetilde{g}_0(n)$ will then be of length 11. Figures 18 and 19 illustrate the analysis and synthesis wavelets respectively, obtained from a symmetric factorization. The first panel of each figure also shows the magnitude of the complex wavelet $|\psi(t)|$ where $\psi(t) = \psi_h(t) + j\,\psi_g(t)$. In the second panel of each figure, the magnitude of the spectrum of the complex wavelet, $|\Psi(\omega)|$, is also shown. These plots of $|\Psi_h(\omega) + j\,\Psi_g(\omega)|$ and likewise $|\widetilde{\Psi}_h(\omega) + j\,\widetilde{\Psi}_g(\omega)|$ show that they approximate zero for $\omega < 0$, which verifies that the two wavelets form an approximate Hilbert pair. The third panel of the figures show a magnification of $|\Psi(\omega)|$ and $|\widetilde{\Psi}(\omega)|$. The dashed line shows $|\Psi(\omega)|$ when a maximally-flat delay polynomial $D(z)$ of degree 2 is used in the design procedure. It can be seen that when the polynomial designed according to the minimax criterion is used, instead of the maximally-flat type, the approximation is substantially improved. For both the analysis and synthesis complex wavelets, the minimax type, $|\Psi(\omega)|$ approximates zero for negative frequencies with substantial improvement — the error is reduced by over a factor of two.

5 Conclusion

Complex Discrete Wavelet Transforms (DWTs) provide three significant advantages for signal processing applications: they have reduced shift sensitivity with low redundancy, improved directionality and explicit phase information. To implement a low-redundancy complex DWT, Selesnick [40, 41] proposed a filter design technique for Kingsbury's Dual-Tree Complex Wavelet Transform [20, 19]. Selesnick's method creates a Hilbert wavelet pair with specified vanishing-moments by spectral factorization of a halfband filter containing a fractional-delay allpass factor. In Section 4, we demonstrate that both orthogonal and biorthogonal wavelet-pairs approximate a Hilbert pair with less than half the error when a minimax fractional-delay allpass factor is used instead of the maximally-flat allpass factor proposed earlier by Selesnick. Because the advantages of complex DWTs arise from the Hilbert-pair relationship, the improvement in approximation implies that the advantages of the low-redundancy dual-tree complex DWT will be more pronounced when minimax allpass systems are incorporated into the design procedure.

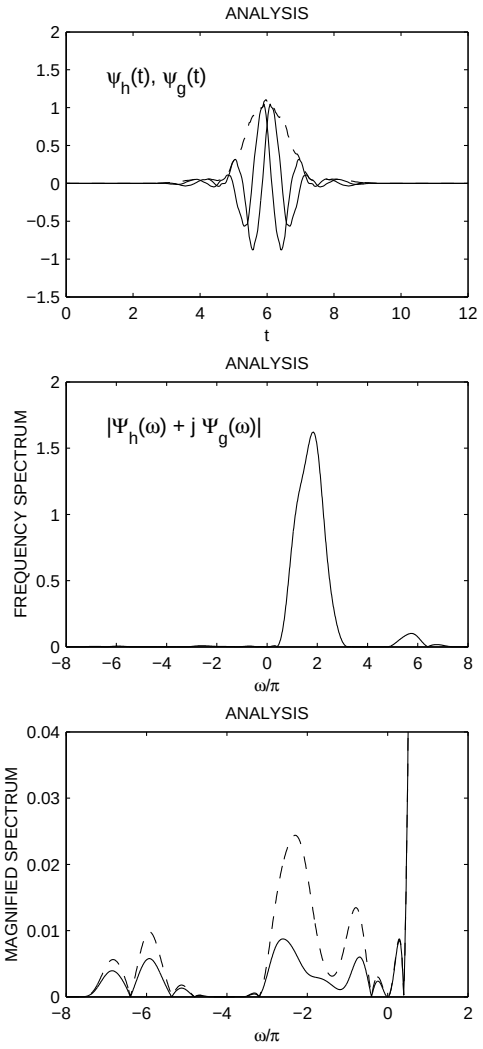

Figure 18: An approximate Hilbert pair of analysis wavelets. The dashed curve in the lower panel illustrates the solution corresponding to a design based on the maximally-flat delay allpass system. The solution obtained with a minimax delay allpass system approximates more accurately the Hilbert pair property.

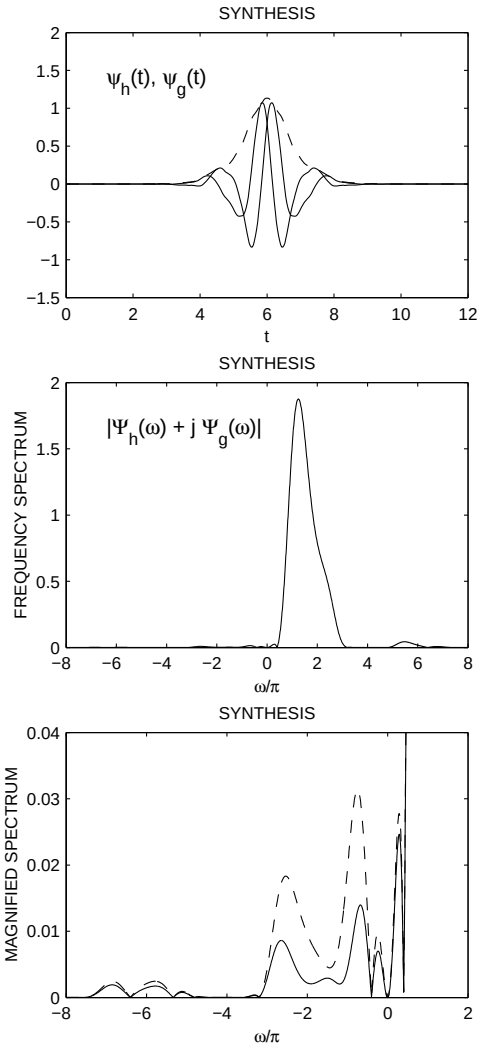

Figure 19: An approximate Hilbert pair of synthesis wavelets. The solution obtained using a maximally-flat allpass illustrated with a dashed line, does not provide as accurate an approximation to the Hilbert pair property as the solution obtained using the minimax allpass system.

In Section 3, we discuss the projection-based approach to complex DWTs. This method allows the implementation of low-redundancy complex DWTs as well as non-redundant complex DWTs. The low-redundancy complex DWT provides the same advantages as the DTWT. On the other hand, the non-redundant complex DWT is a parsimonious signal representation with improved directionality and explicit phase information. In particular, it is useful in applications such as image/video compression, where parsimonious signal representations are crucial. In earlier research, Fernandes [7] showed that the non-redundant complex DWT is orthogonal if the associated projection filter is generated by the modulation of a lowpass filter that is the sum of allpass polyphase components with fractional delay. In Section 3.2, we demonstrate that the directionality of the non-redundant complex DWT is visibly improved by using minimax allpass filters instead of maximally flat allpass filters in the projection-filter design.

To conclude, we emphasize that both low-redundancy complex DWTs and non-redundant complex DWTs may be designed with fractional-delay allpass systems. These complex DWTs offer several significant advantages to signal processing applications. In both transforms, these advantages are more pronounced when minimax fractional-delay allpass systems are used instead of maximally flat fractional-delay allpass systems.

References

[1] M. S. Anderson and S. S. Lawson. Direct design of approximately linear phase (ALP) 2-D IIR digital filters. *Electron. Lett.*, 29(9):804–805, 29th April 1993.

[2] R. Ansari and B. Liu. A class of low-noise computationally efficient recursive digital filters with applications to sampling rate alterations. *IEEE Trans. on Acoust., Speech, Signal Proc.*, 33(1):90–97, February 1985.

[3] C. S. Burrus, R. A. Gopinath, and H. Guo. *Introduction to Wavelets and the Wavelet Transform - A Primer*. Prentice-Hall, 1998. Expansion of notes for the IEEE Signal Processing Society's tutorial program held in conjunction with the ICASSP-93 on April 26, 1993.

[4] C.-K. Chen and J.-H. Lee. Design of digital all-pass filters using a weighted least squares approach. *IEEE Trans. on Circuits and Systems II*, 41(5):346–351, May 1994.

[5] I. Daubechies. *Ten Lectures On Wavelets*. SIAM, 1992.

[6] P. de Rivaz and N. Kingsbury. Complex wavelet features for fast texture image retrieval. In *IEEE Proc. Int. Conf. Image Processing*, 1999.

[7] F. C. A. Fernandes. *Directional, Shift-Insensitive, Complex Wavelet Transforms with Controllable Redundancy*. PhD thesis, Rice University, January 2002. http://www.ece.rice.edu/-felixf/dissertation.pdf.

[8] F. C. A. Fernandes, R. van Spaendonck, M. Coates, and C. S. Burrus. Directional complex-wavelet processing. In *Wavelet Applications VII, Proceedings of SPIE*, 2000.

[9] A. Fettweis. A simple design of maximally flat delay digital filters. *IEEE Trans. Audio Electroacoust.*, 20:112–114, June 1971.

[10] M. Gerken. Allpass transfer functions with prescribed group delay. In *Proc. IEEE Int. Conf. Acoust., Speech, Signal Processing (ICASSP)*, volume 3, pages 577–580, Adelaide, April 19-22 1994.

[11] M. Gerken, H. W. Schüßler, and P. Steffen. On the design of digital filters consisting of a parallel connection of allpass sections and delay elements. *Archiv für Electronik und Übertragungstechnik (AEÜ)*, 49(1):1–11, January 1995.

[12] R. Gopinath. The phaselet transform - an integral redundancy nearly shift-invariant wavelet transform. 2001. preprint.

[13] G. H. Granlund and H. Knutsson. *Signal Processing for Computer Vision*. Kluwer Academic Publishers, 1995.

[14] T. Henk. New algorithm for maximally-flat, lowpass delay approximation. In *Proceedings of the European Conf. on Circuit Theory and Design*, pages 658–661, 1985.

[15] M. Ikehara, H. Tanaka, and H. Kuroda. Design of IIR filters using all-pass networks. *IEEE Trans. on Circuits and Systems II*, 41(3):231–235, March 1994.

[16] B. Jaworski and T. Saramäki. Linear phase IIR filters composed of two parallel allpass sections. In *Proc. IEEE Int. Symp. Circuits and Systems (ISCAS)*, volume 2, pages 537–540, London, May 30-June 2 1994.

[17] Z. Jing. A new method for digital all-pass filter design. *IEEE Trans. on Acoust., Speech, Signal Proc.*, 35(11):1557–1564, November 1987.

[18] S. S. Kidambi. Weighted least-squares design of recursive allpass filters. *IEEE Trans. on Signal Processing*, 44(6):1553–1556, June 1996.

[19] N. Kingsbury. Complex wavelets for shift invariant analysis and filtering of signals. *Applied and Computational Harmonic Analysis*, June 2000.

[20] N. G. Kingsbury. Image processing with complex wavelets. *Phil. Trans. Royal Society London A*, September 1999.

[21] T. I. Laakso, V. Välimäki, M. Karjalainen, and U. K. Laine. Splitting the unit delay. *IEEE Signal Processing Magazine*, 13(1):30–60, January 1996.

[22] M. Lang. Allpass filter design and applications. In *Proc. IEEE Int. Conf. Acoust., Speech, Signal Processing (ICASSP)*, volume 2, pages 1264–1267, Detroit, May 9-12 1995.

[23] M. Lang. Allpass filter design and applications. *IEEE Trans. on Signal Processing*, 46(9):2505–2514, September 1998.

[24] M. Lang and T. Laakso. Simple and robust method for the design of allpass filters using least-squares phase error criterion. *IEEE Trans. on Circuits and Systems II*, 41(1):40–48, January 1994.

[25] S. Lawson. A new direct design technique for ALP recursive digital filters. In *Proc. IEEE Int. Symp. Circuits and Systems (ISCAS)*, volume 1, pages 499–502, Chicago, May 3-6 1993.

[26] K. Matsuyama, M. Okuda, and M. Ikehara. Approximation of group delay response using weighted least square method. In *Proc. IEEE Int. Symp. Circuits and Systems (ISCAS)*, volume 2, pages 197–200, Atlanta, May 12-15 1996.

[27] T. Q. Nguyen, T. I. Laakso, and R. D. Koilpillai. Eigenfilter approach for the design of allpass filters approximating a given phase response. *IEEE Trans. on Signal Processing*, 42(9):2257–2263, September 1994.

[28] S.-C. Pei and J.-J. Shyu. Eigenfilter design of 1-D and 2-D IIR digital all-pass filters. *IEEE Trans. on Signal Processing*, 42(4):966–968, April 1994.

[29] S.-C. Pei and C.-C. Tseng. Two novel methods for complex allpass filters design using remez exchange algorithm. In *Proc. IEEE Int. Symp. Circuits and Systems (ISCAS)*, volume 2, pages 173–176, Atlanta, May 12-15 1996.

[30] S.-M. Phoong, C. W. Kim, P. P. Vaidyanathan, and R. Ansari. A new class of two-channel biorthogonal filter banks and wavelet bases. *IEEE Transactions on Signal Processing*, 43(3):649–665, March 1995.

[31] M. Renfors and T. Saramäki. A class of approximately linear phase digital filters composed of allpass subfilters. In *Proc. IEEE Int. Symp. Circuits and Systems (ISCAS)*, volume 2, pages 678–681, San Jose, May 5-7 1986.

[32] J. K. Romberg, H. Choi, R. G. Baraniuk, and N. G. Kingsbury. Hidden Markov tree models for complex wavelet transforms. *IEEE Transactions on Signal Processing*, 2001 (submitted).

[33] T. Saramäki. On the design of digital filters as a sum of two all-pass filters. *IEEE Trans. on Circuits and Systems*, 32(11):1191–1193, November 1985.

[34] H. W. Schuessler and P. Steffen. Recursive halfband-filters. *International Journal of Electronics and Communications*, 55(6):1–12, 2001.

[35] H. W. Schüssler and P. Steffen. Some advanced topics in filter design. In J. S. Lim and A. V. Oppenheim, editors, *Advanced Topics in Signal Processing*, chapter 8, pages 416–491. Prentice Hall, 1988.

[36] H. W. Schüßler and P. Steffen. On the design of allpasses with prescribed group delay. In *Proc. IEEE Int. Conf. Acoust., Speech, Signal Processing (ICASSP)*, volume 3, pages 1313–1316, Albuquerque, April 3-6 1990.

[37] H. W. Schüßler and P. Steffen. Halfband filters and Hilbert transformers. *Circuits, Systems, and Signal Processing*, 17(2):137–164, 1998.

[38] H. W. Schüssler and J. Weith. On the design of recursive Hilbert-transformers. In *Proc. IEEE Int. Conf. Acoust., Speech, Signal Processing (ICASSP)*, volume 2, pages 876–879, Dallas, April 6-9 1987.

[39] I. W. Selesnick. Lowpass filters realizable as allpass sums: design via a new flat delay filter. *IEEE Trans. on Circuits and Systems Part II*, 46(1):40–50, January 1999.

[40] I. W. Selesnick. Hilbert transform pairs of wavelet bases. *IEEE Signal Processing Letters*, 8(6):170–173, June 2001.

[41] I. W. Selesnick. The design of approximate Hilbert transform pairs of wavelet bases. *IEEE Trans. on Signal Processing*, 50(5):1144–1152, May 2002.

[42] I. W. Selesnick and L. Sendur. Iterated oversampled filter banks and wavelet frames. In *Wavelet Applications VII, Proceedings of SPIE*, 2000.

[43] S. Signell. Design of maximally flat group delay discrete-time recursive filters. In *Proc. IEEE Int. Symp. Circuits and Systems (ISCAS)*, volume 1, pages 193–196, Montreal, May 7-10 1984.

[44] M. J. T. Smith and T. P. Barnwell III. Exact reconstruction for tree-structured subband coders. *IEEE Trans. ASSP*, 34(3):431–441, June 1986.

[45] G. Strang and T. Nguyen. *Wavelets and Filter Banks*. Wellesley-Cambridge Press, Wellesley, MA, 1996.

[46] J. P. Thiran. Recursive digital filters with maximally flat group delay. *IEEE Trans. on Circuit Theory*, 18(6):659–664, November 1971.

[47] P. P. Vaidyanathan. *Multirate Systems and Filter Banks*. Prentice Hall, 1993.

[48] X. Zhang and H. Iwakura. Novel method for designing digital allpass filters based on eigenvalue problem. *Electron. Lett.*, 29(14):1279–1281, 8th July 1993.